Current Optics and Photonics
Vol. 3, No. 2, April 2019, pp. 154-163

ISSN: 2508-7266(Print) / ISSN: 2508-7274(Online)
DOI: https://doi.org/10.3807/COPP.2019.3.2.154

Development of Optical Sighting System for Moving Target Tracking

Bo-Sun Jeung[1], Sung-Soo Lim[2], and Dong-Hee Lee[3]*

[1]*Department of Information & Telecommunication, Graduate School of Far East University, Gamgok 27601, Korea*
[2]*Research Center of DongIn Optical Co. Ltd., Bucheon 14450, Korea*
[3]*Department of Visual Optics, Far East University, Gamgok 27601, Korea*

(Received November 21, 2018 : revised December 5, 2018 : accepted December 11, 2018)

In this study, we developed an optical sighting system capable of shooting at a long-distance target by operating a digital gyro mirror composed of a gyro sensor and an FSM. The optical sighting system consists of a reticle part, a digital gyro mirror (FSM), a parallax correction lens, a reticle-ray reflection mirror, and a partial reflection window. In order to obtain the optimal volume and to calculate the leading angle range according to the driving angle of the FSM, a calculation program using Euler rotation angles and a three-dimensional reflection matrix was developed. With this program we have confirmed that the horizontal leading angle of the developed optical sighting system can be implemented under about ±8° for the maximum horizontal driving angle ($\beta = \pm 12.5°$) of the current FSM. Also, if the β horizontal driving angle of the FSM is under about ±15.5°, it can be confirmed that the horizontal direction leading angle can be under ±10.0°. If diagonal leading angles are allowed, we confirmed that we can achieve a diagonal leading angle of ±10.0° with a vertical driving angle α of ±7.1° and horizontal driving angle β of ±12.5°.

Keywords : Optical sighting system, Leading angle, FSM, 3D reflection matrix
OCIS codes : (220.0220) Optical design and fabrication; (220.2740) Geometric optical design; (220.4830) Systems design; (220.4880) Optomechanics

I. INTRODUCTION

On conventional moving target tracking devices there is a mechanical sighting device and an optical sighting device. The mechanical sighting device is made easily by anyone who can do a little survey and research because the technique has been disclosed [1, 2]. However, in modern times, as moving targets speed up, the tracking speed of such a device has been unable to follow the moving targets. So, this device is not used well. However, as a moving target tracking device, optical sighting devices are still used for tracking armored vehicles, low-speed planes, helicopters and marine speedboats. In particular, the Vulcan may be a good application case of an optical sighting device in the military field. The Vulcan is a rapidly destructive weapon designed to launch 6,000 shots per minute, in which the tracking of moving targets is essential. In particular, to attack long-distance targets, the Vulcan has to calculate the leading angle of the target and then fire at it. It is difficult to increase the precision by manual operation in order to aim with the leading angle according to the moving speed of the target. So, for automatic adjustment, an analog gyro mirror has been applied to create a leading angle. However, since the analog gyro mirror is bulky and has a long initial driving time, it takes a considerable amount of time even in a situation where fast responses are required.

The optical sighting device for the Vulcan, which is capable of moving target tracking, is a device that combines an electro-mechanics system that connects a digital actuating mirror and a gyro sensor, and an optical sighting system. This combined technology is known as a kind of special technology that is not transferred to other countries.

However, in Korea, an optical dot-sight system similar to the optical sighting system for the Vulcan has already been

*Corresponding author: dhlee99@hanafos.com, ORCID 0000-0001-7655-0058
Color versions of one or more of the figures in this paper are available online.

studied extensively [3-6]. And recently, a digital mirror called a Fast Steering Mirror (FSM) has been developed [7-10] and is widely used in fields such as laser optics and fine adjustment technology. By attaching a gyro sensor chip to the FSM, it can act as a good gyro mirror. Therefore, in this paper, we wanted to develop an optical sighting system for the Vulcan that uses the FSM combined with the gyro sensor.

II. DESIGN OF OPTICAL SIGHTING SYSTEM FOR MOVING TARGET TRACKING

2.1. Initial Configuration of the Optical Sighting System

The proposed optical sighting system consists of a reticle part, a digital gyro mirror (FSM), a parallax correction lens, a reticle-ray reflection mirror that reflects rays from the FSM onto the parallax correction lens, and a partial reflecting window. The reticle part is composed of two devices, i.e., an illumination device with a red light (central wavelength; 658 nm) LED as a light source and a mask reticle that is used to create a virtual image reticle for target tracking by being projected by the illumination device. Also, the partial reflective window allows the light rays from the outer target to be transmitted to the observer and the light rays from the inner reticle part to reflect to the observer so that the observer can simultaneously see the virtual image of the mask reticle and the external target at the external target position. Figure 1 shows a front view and the observed optical structure of the optical sighting system of the old model GSA-MK3 that we want to improve. This observed structure allows us to identify the development components we need, as described above.

2.2. Importance of Leading Angle in Moving Target Tracking

A long time ago, a leading angle was used in ballistics to hit a moving object. The leading angle at this time is to make the barrel move forward slightly in the direction in which the target moves in order to hit the moving target. However, in the optical sighting system, the leading angle has been used to hit a moving fighter since the development of the combat plane, and so far, there has been no optical theory and technology disclosure in this field to protect the technology.

The role of the leading angle in most optical sighting systems can be seen in Fig. 2. First, steps (a) and (b) are to track the target so that the reticle of the optical sighting system seen by the observer matches the moving target. At this time, the gyro sensor calculates the moving speed of the target by sensing the moving angular velocity of the target. In step (c), the MCU computes the leading angle of the Vulcan barrel based on the moving speed of the target detected in steps (a) and (b) and commands the FSM to back up the reticle as much as the leading angle. In step (d), the observer again aligns the retracted reticle with the target and fires it. When the reticle in step (c) is matched to the target as in step (d), the optical sighting system must be rotated toward the target as much as the leading angle, so that the Vulcan barrel, moving in accordance with the optical sighting system, is positioned ahead of the target by the leading angle. By doing this, we can hit the moving target. But what is important here is to figure out what the required leading angle is when you know the speed of the plane you are going to hit, and the size of the observation window. It is also important to know the driving angle of the FSM to realize this leading angle.

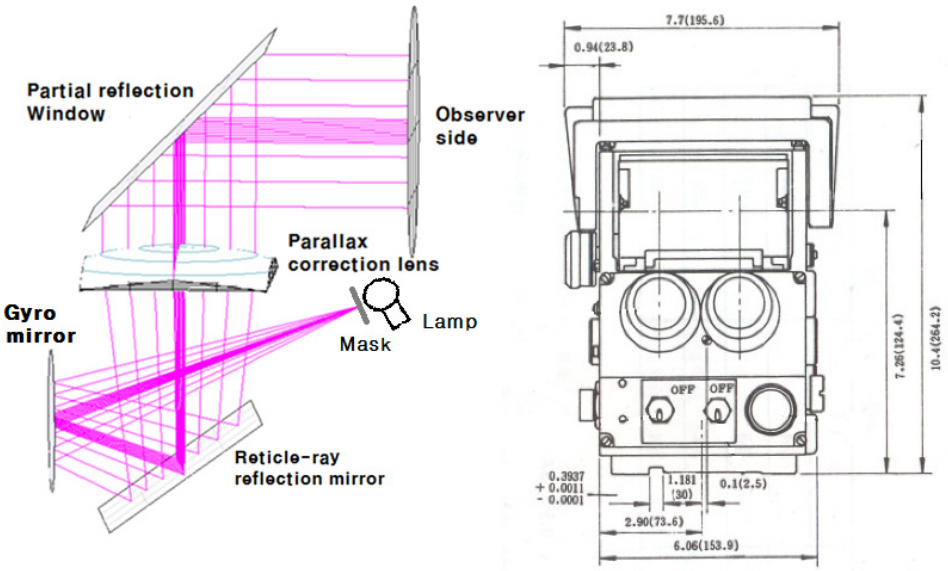

FIG. 1. Front view and optical structure of the GSA-MK3 optical sighting system (Since the GSA-MK3 actually uses one window for both moving target tracking and fixed target tracking, the half of the window shown in the figure can be judged as the window for moving target tracking).

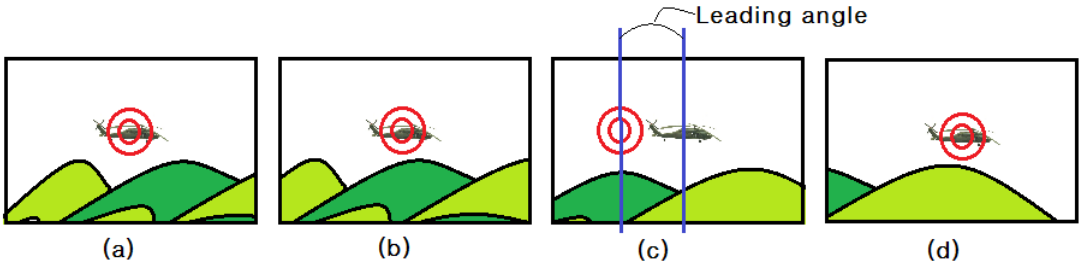

FIG. 2. Diagram showing the role of the leading angle in the optical sighting system.

But until now, an optical theory and program on how to determine the maximum leading angle when the size of the observation window of the optical sighting system is given, as well as how much the horizontal and vertical rotation angles of the FSM are required to have a specific leading angle, has not been developed. In this paper, we tried to describe them.

2.3. Derivation of the Image Position of the Reticle Reflected by the α and β Driving Angles of the FSM

The role of the FSM we adopted is to cause the principal ray from the reticle to the center of the parallax correction lens to be incident at a specific angle on the optical axis of the parallax correction lens. So, if we omit the reticle-ray reflection mirror and set the coordinate system considering only the principal ray path, the reticle, the FSM, and the parallax correction lens, the whole system becomes simple, as shown in Fig. 3. Figure 3 shows that the XYZ coordinate system is set based on the FSM center and that the two rotation axes of the FSM, which are orthogonal to each other, rotate by the α and β driving angles, which are the Euler rotation angles [11]. When the two rotation axes of the FSM rotate, the principal ray directing from the reticle to the first principal point of the parallax correction lens also moves while drawing a similar trajectory as the oblique plane of the cone, with the principal point of the parallax correction lens as the vertex and the optical axis of the parallax correction lens as the central axis. This motion of the reticle's principal ray induced by the reflection of the FSM is required for inducing the movement of the visual axis to the target by which the optical sighting system can track the target, and for deriving the leading angle necessary for distant shooting.

For these tasks, it is necessary to calculate how much the reflected image of the reticle caused by the moving of the FSM moves in the Y′Z′ plane of Fig. 3 when the two rotation axes of the FSM are rotated at Euler angles α and β. Then the normal direction transformation of the reflection surface of the FSM according to the change of the Euler angles should be obtained first. If the unit normal vector (-1, 0, 0) direction of the FSM is initially in the X-axis direction in Fig. 3, the unit normal direction of the FSM according to the α and β of the Euler rotation angles [11-13] will be changed as follows.

$$\begin{bmatrix} a \\ b \\ c \end{bmatrix} = \begin{bmatrix} -\cos\alpha\cos\beta \\ -\sin\alpha \\ \cos\alpha\sin\beta \end{bmatrix} \tag{1}$$

Therefore, the surface equation of the FSM passing through the origin of the coordinate system as shown in Fig. 3 can be expressed as follows.

$$ax + by + cz = 0 \tag{2}$$

If the unit normal vector of the reflected surface of the rotated FSM is given by (a, b, c), the position shift of the reflection image of the reticle by the rotated FSM can be obtained by the following three-dimensional (3D) reflection matrix [14, 15].

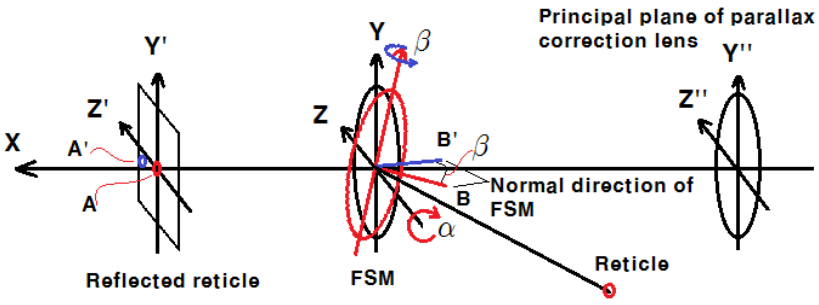

FIG. 3. Diagram on deriving the deviation angle of the principal ray connecting the reticle and the first principal point of the parallax correction lens from the optical axis of the parallax correction lens as the FSM rotates according to the Euler rotation angles.

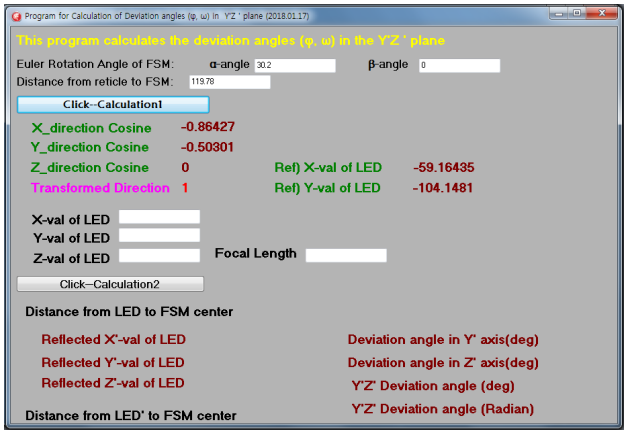

FIG. 4. An example of the first step program execution results that shows the position coordinates of the reflection reticle determined when the normal axis of the FSM mirror is α = 30.2° (Δα = 0°) and β = 0°.

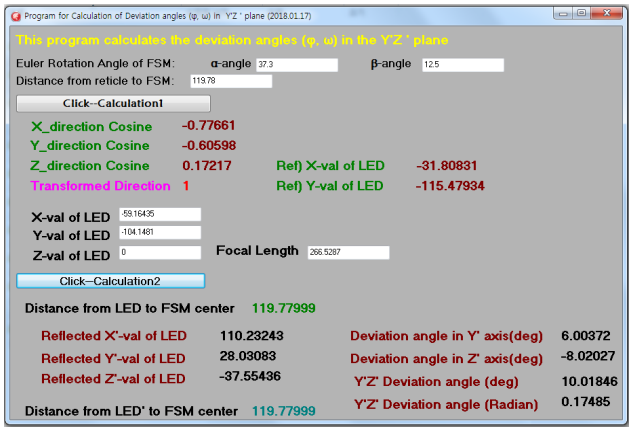

FIG. 5. An example of the second step program execution results that shows the deviation angle coordinates of the reflection reticle determined when the normal axis of the FSM mirror is α = 37.3° (Δα = 7.1°) and β = 12.5°.

$$\begin{bmatrix} x' \\ y' \\ z' \end{bmatrix} = \begin{bmatrix} 1-2a^2 & -2ab & -2ac \\ -2ab & 1-2b^2 & -2bc \\ -2ac & -2bc & 1-2c^2 \end{bmatrix} \begin{bmatrix} x \\ y \\ z \end{bmatrix} \quad (3)$$

where (x′, y′, z′) is the position value of the XY′Z′ coordinate system in Fig 2.

Then, the deviation angles (φ, ω) in the Y′Z′ plane of Fig. 3 deviated from the optical axis of the parallax correction lens of the reticle image reflected by the rotated FSM are expressed as follows.

$$\varphi \text{ (deviation angle in the Y}' \text{ direction)} = \tan^{-1}\left(\frac{y'}{f' - \Delta\sigma}\right) \quad (4)$$

$$\omega \text{ (deviation angle in the Z}' \text{ direction)} = \tan^{-1}\left(\frac{z'}{f' - \Delta\sigma}\right) \quad (5)$$

where f′ is the effective focal length of the parallax correction lens, σ is the distance from the center of FSM to the reticle, and Δσ = σ - x′.

These angles, φ and ω, are required to calculate the leading angle of the distant target and the visual axis angle to the target.

Therefore, we could use the Euler rotation angles and the above 3D reflection matrix to develop a program such as in Figs. 4 and 5 to calculate the leading angle range and the visual axis angle range according to the FSM driving angle, as well as to obtain the optimal volume.

2.4. Design of the Optical Sighting System

The appearance and specifications of the FSM to be applied to our optical system are shown in Table 1 and Fig. 6. In contrast to the effective diameter of the GSA-MK3 of 31.8 mm, the effective diameter of the newly adopted FSM of 50.8 mm means that the range of effective rays to be transmitted from the reticle to the parallax correction lens is widened. This indicates that the new model can achieve a wider leading angle than the GSA-MK3.

In Fig. 6, we can see that the driving axis of the FSM is set so that the driving angle of the FSM becomes the α and β of Euler angles.

The condition that the volume of the development product should not be larger than that of the existing

TABLE 1. Optical and physical characteristics of the FSM used in the development of our product

Parameter	Values
Mirror aperture size (mm)	50.8 mm (2 inches)
FSM angular velocity (degree/sec)	10
FSM module volume (mm)	Max. 122 × 112 × 92
Angular tilt	α = ±12.5 degrees, β = ±12.5 degrees
Controller type	Digital FPGA
Mirror condition	PV < 1/6 wave, RMS < 0.047 wave@630 nm
Coating	R ≥ 95.0% @ 650 nm ± 40 nm
Accuracy	3~4 μrad

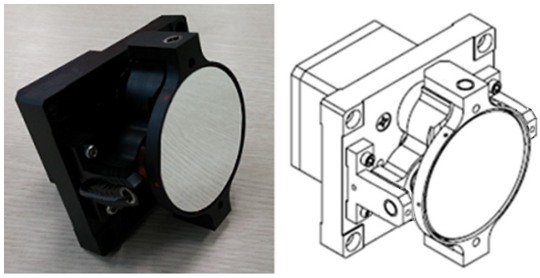

FIG. 6. Appearance of the FSM to be applied to our optical system.

GSA-MK3 was given by the development sponsor. So, we analyzed the existing products as much as possible so that the total volume is not larger than that of the existing GSA-MK3, while the area where the reticle's virtual image is seen in the window is larger than the GSA-MK3. Because the GSA-MK3 uses moving target tracking and fixed-target tracking together in one window, the window used only for the moving target tracking is almost the same as half of the window shown outside. On the other hand, in our system, all parts of the window shown from the outside are used for the tracking of the moving target or for the tracking of the fixed target, if necessary. This is accomplished by placing a reticle mask for moving target tracking and a reticle mask for fixed-target tracking on two adjacent sides of a cubic beam-splitter (shown in Fig. 7) with a 50% reflective layer on the inner diagonal bevel [4, 6, 16]. That is, if necessary, the reticle mask for moving target tracking or for fixed target tracking may be used. Then, the user can use all parts of the window that are seen from the outside for both moving target tracking and fixed target tracking. Also, in order to enlarge the area where the reticle's virtual image is seen in the window, the size of the lens should be made larger than that of the GSA-MK3.

In order to optimize the volume so that the total volume is not larger than that of the existing GSA-MK3 and the leading angle can be larger than that of the existing GSA-MK3, the optimal space should be calculated by simulating the space for the placement of each component by using the above-mentioned Eqs. (1) to (5). To do this, we developed a program as shown in Fig. 4 and used it to optimize the space. That is, the program is configured by the step of calculating the reflection coordinate of the reticle image by inputting the rotation angle of the FSM as aninitial arrangement angle α of the optical sighting system (generally, this angle is half of the bending angle of the FSM, as shown in Table 2), and the step of calculating the deviation angle that is deviated from the optical axis of the parallax correction lens of the reflected reticle image by inputting the effective focal length of the whole system and the driving angles of the FSM. Here we need to know that this angle serves as the leading angle in target tracking. Examples of the execution of the program

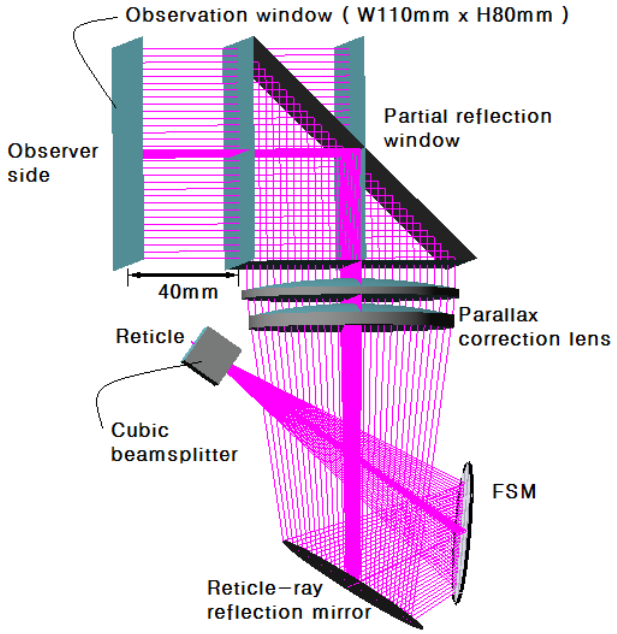

FIG. 7. Configuration of the optimized optical sight system (with Euler angles of $\alpha = 30.2°$ ($\Delta\alpha = 0°$) and $\beta = 0$).

in each step are shown in Figs. 4 and 5. Figure 4 shows the coordinate values of the reticle in the coordinate system XYZ such that the virtual image of the reticle is placed on the optical axis of the parallax correction lens at the initial arrangement angle α of the FSM. Figure 5 shows the calculated deviation angle of the reflected reticle image that is deviated from the optical axis of the parallax correction lens, when the FSM is operated by $\Delta\alpha = 7.1°$ and $\beta = 12.5°$ of Euler angles (that is, the angle that drives the FSM for tracking the actual target). Using this program, we were able to obtain a system as in Table 2 and Fig. 7 optimized for a volume of 264 mm × 292 mm × 196 mm and $\alpha = 30.2°$ tilting angle of the normal vector of the FSM. This means that the optimization was done in the direction of increasing the optical capacity of the internal components so as to maintain a leading angle of about 10° without being larger than the volume of the GSA-MK3. Also, this is the result of adopting the FSM shown in Fig. 6, a new gyro mirror that is smaller in volume and larger in mirror size than the gyro mirror of the existing GSA-MK3, and adopting a small volume LED as a light source.

III. DISCUSSION OF DESIGN RESULTS

Figure 7 and Tables 2 and 3 show that the structure of the optimized optical sighting system is not larger than that of the GSA-MK3 and the size of the partial reflection window for moving target tracking, in which the external target and the virtual image of the reticle are overlapped, is not smaller than that of the GSA-MK3. But, as mentioned before, using the new optical component, i.e., the cubic

TABLE 2. Design data of the optimized optical sighting system (In the table below, the bending angle refers to the angle by which the optical axis of the parallax correction lens is bent at each reflection surface)

Surface	Radius (mm)	Thickness (mm)	Remark (Bending angle, Diameter or H × W)
Object	Infinity	2.050	
1	Infinity	15.000	BK7: Cubic beam-splitter
2	Infinity	102.730	
3	Infinity	-43.710	Reflect: FSM (60.4°, 50.4 mm)
4	Infinity	94.816	Reflect: Reticle-ray reflection mirror (64.9°, 60 mm)
Stop	-230.3916	6.000	BK7: Parallax correction lens1 (78 mm)
6	-161.6277	2.000	
7	Infinity	7.000	BK7: Parallax correction lens2
8	-185.8186	2.000	(78 mm)
9	Infinity	43.000	
10	Infinity	-40.000	Reflect: Partial reflection window (80 mm × 110 mm)
11	Infinity	-40.000	
Image	Infinity	0	Focal length: 266.5287 mm

TABLE 3. Comparison of the appearance size and the window size of the optimized system and the GSA-MK3

	GSA-MK3	Optimized system
Volume (H × L × W)	264 mm × 292 mm × 196 mm	264 mm × 292 mm × 196 mm
Observation window (H × L)	80 mm × 110 mm	80 mm × 110 mm
FSM (dia.)	31.8 mm	50.4 mm
Parallax correction lens (dia.)	51.3 mm	78 mm

beam-splitter, we can use the partial reflection window of the developed product more widely in the tracking of a moving object or the tracking of a stopped object than the existing GSA-MK3, even though the same size partial reflection window is used.

Figure 8 shows the distribution of the parallax amount of the effective aperture of 78.0 mm of the parallax correction lens designed optimally. Since the maximum parallax is 1.659 minutes at a reticle distance of 266.529, it means that the aiming difference between the virtual image of the reticle projected on the target and the target

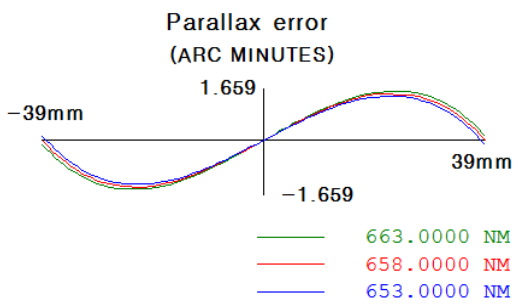

FIG. 8. Parallax error distribution of the parallax correction lens of the optimized optical sighting system.

is up to 1.659 minutes. In other words, it means that the aiming error is ±1000 m × $\tan\left(\frac{1.659}{60}\right)$ ≅ ±48 cm when aiming at an object that is about 1 km away.

If we know the α and β angles, we can calculate the angles of deviation of the principal ray of the reticle (ultimately, this becomes the visual axis of tracking the target) off the center axis of the observation window with the execution of the program in Fig. 5. If the angles of deviation of the principal ray are set to a_y in the y‴-axis direction and a_z in the z‴-axis direction in the xy‴z‴ coordinate system, we can then obtain the deviation angle a_y and a_z, as shown in Table 4. In the simulation in Fig. 9, we can see the range of visual axis angles of the target where the virtual image of the reticle is superimposed when the driving of the α and β Euler angles of the FSM is implemented. When the FSM is driven vertically, Figs. 9(a) and 9(b) show the range of the α driving angle of the FSM. That is, these show the range of the α driving angle from which the rays of the reticle can be passed into the observation window set to a size of 110 mm (horizontal) × 80 mm (vertical) in front of 40 mm of the partial reflection window, as shown in Fig. 9(c). Figures 9(c)~9(e) show that when the β angle, which is the horizontal driving

angle of the FSM, increases to 18.5°, the reticle rays pass through the observation window. That is, when the β angle exceeds 18.5°, it indicates that the light rays from the reticle can't pass through the observation window. From the above, it can be seen that the FSM driving angle of the developed optical sighting system is from 12.20° to -12.30° in the α angle only, and ±18.50° in the β angle only. The corresponding deviation angles of the visual axis of the target from the optical axis of the observation window are shown in Table 4 as 10.60~-10.75 in the vertical direction and a_z (±11.71°) & a_y (0°~-0.57°) in the horizontal direction, respectively. However, since the β

TABLE 4. Deviation angles of the virtual image of the reticle calculated by the program in Fig. 5 corresponding to the α and β Euler angles of the FSM in Fig. 9

Figure # in Fig. 9	Δα (°)	β (°)	a_y (°)	a_z (°)	Dia (°)
(a)	12.20	0.00	10.60	0.00	10.60
(b)	-12.30	0.00	-10.75	0.00	10.75
(c)	0.00	12.50	-0.26	-8.17	8.18
(d)	0.00	15.50	-0.40	-9.99	10.00
(e)	0.00	18.50	-0.57	-11.71	11.74
(f)	7.10	12.50	6.00	-8.02	10.02
(g)	-7.10	12.50	-6.51	-7.99	10.31

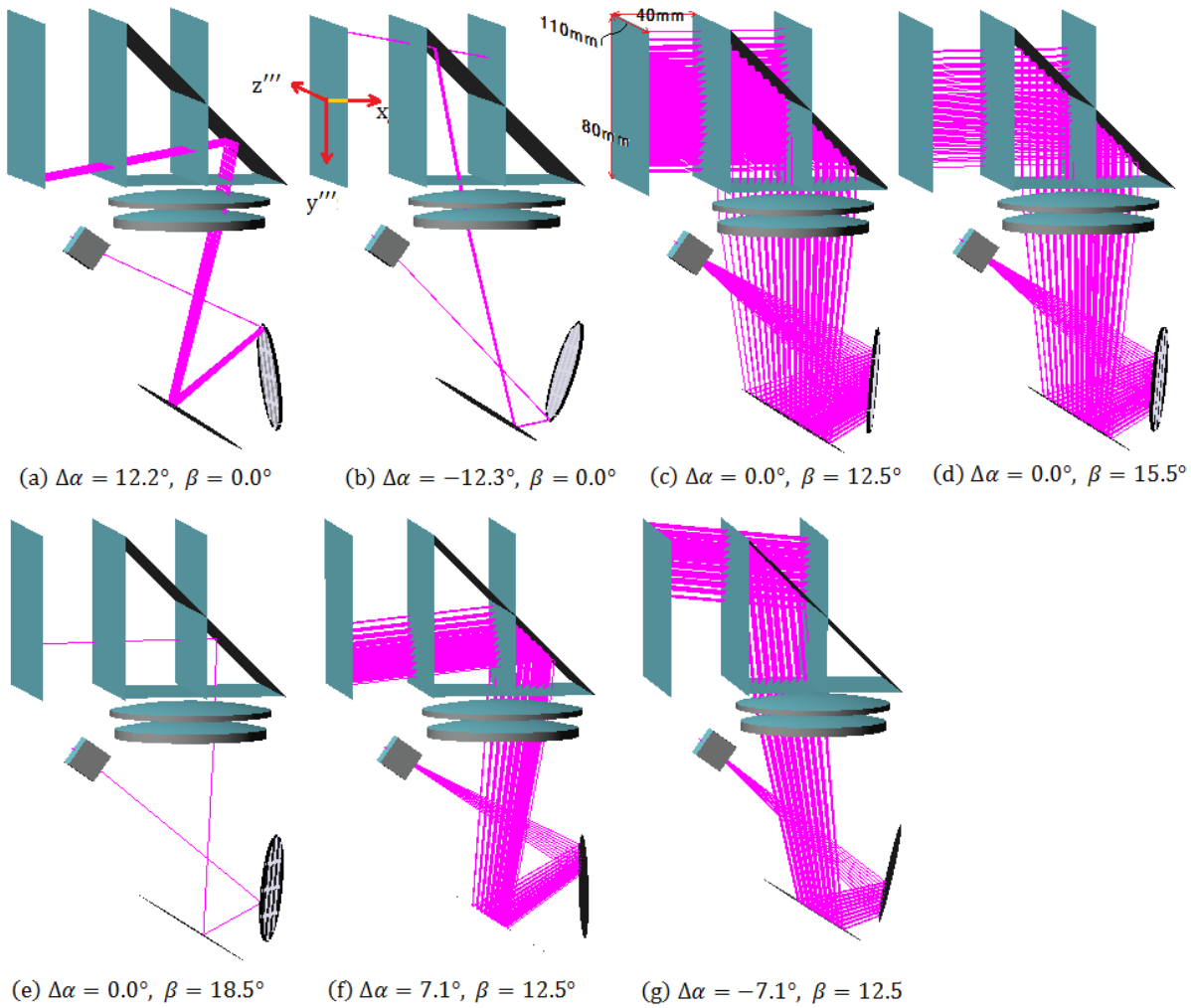

FIG. 9. Simulations showing to what extent the virtual image of the reticle can be formed in the observer's field of view according to the α and β Euler angles of the FSM.

driving range of the currently adopted FSM is ±12.5°, the allowed deviation angles of the visual axis from the optical axis of the observation window are ∓8.17° for a_z and 0°~-0.26° for a_y, as shown in Table 4. In Figs. 9(f), 9(g) and Table 4 we show the driving range of the α and β angles of the FSM for realizing a deviation angle of 10 degrees with the FSM adopted in the developed optical sighting system. That is, if an α angle of ±7.10° and β angle of ±12.5° are implemented, we could know whether it is possible to maintain the diagonal deviation angle of 10, though not the horizontal deviation angle.

These deviation angles can be used as the leading angles if the developed optical sighting system is used for shooting a moving object. For example, in order to shoot a moving object in the horizontal direction, it is first necessary to know the lead angle calculated by the velocity of the bullet, the drop motion by gravity, the shooting distance, and the like. Next, the calculated leading angle should be transmitted to the optical sighting system to drive the α and β angles of the FSM so that the virtual image of the reticle follows the target as late as the transmitted leading angle. The shooter then must match the late virtual image of the reticle to the moving target to get the correct aim again, which causes the gun to be ahead of the target.

Figure 10 shows a block diagram for the FSM driver that calculates the visual axis angle and the leading angles with the digital gyro data from the gyro sensor on the MCU and transfers the drive values to the FSM. Figure 11 shows a sectional view of the developed optical sighting system showing the relative positions of optical components.

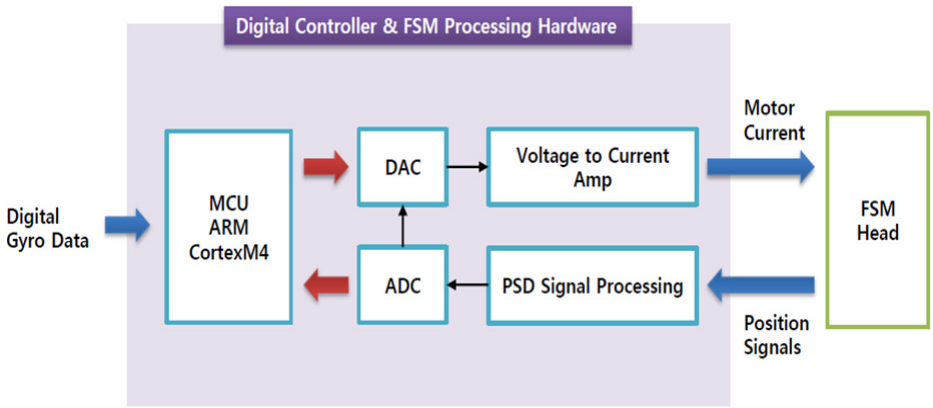

FIG. 10. Block diagram for the FSM driver that calculates the visual axis angle and the leading angles with gyro data from the gyro censer on the MCU and transfers the drive values to the FSM.

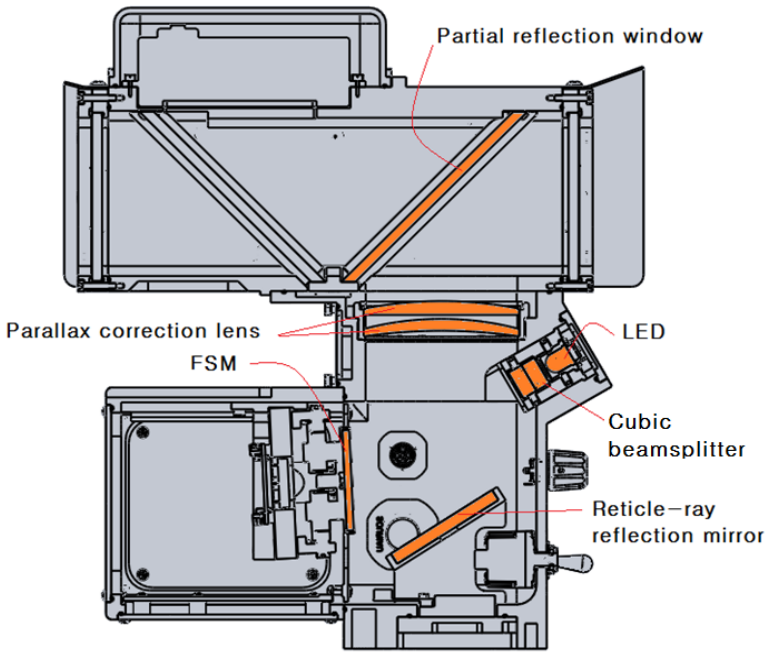

FIG. 11. Sectional view of the developed optical sighting system showing the relative positions of optical components.

FIG. 12. Appearances of the developed optical sighting system.

Figure 12 shows the appearances of the developed optical sighting system. On the right side of Fig. 12 is the photograph of the actual developed product and on the left is the CAD picture of the developed product. Figure 13 is the photographs showing the projected states of the reticle for the fixed-target tracking and the reticle for the moving target tracking on two adjacent sides of the cubic beam-splitter. Figure 14 shows photographs depicting how an external object and virtual image of the reticle can be seen in a superimposed state anywhere on the observation window in the developed optical sighting system. This has the same characteristics as a dot sighting system [3-6, 17]. That is, the existing dot sighting system has the characteristics that when the virtual image of the dot reticle and the outside target overlap and are fired anywhere in the observation window of the dot sighting system, the target can be hit. However, since the developed optical sighting system has a digital gyro mirror composed of an FSM and a gyro sensor, it is a device that can easily hit a long-distance target if it calculates and reflects a proper leading angle to the target.

IV. CONCLUSION

In this paper, we have designed an optical sighting system that can induce a leading angle by using a digital gyro mirror composed of a gyro sensor and an FSM. Here we need to calculate the optimum volume and the range of the optimal leading angle. So, we solved this problem by using a program developed using Euler rotation angles and a 3D reflection matrix.

Until now, an optical theory and program on how to determine the leading angle when the size of the observation

FIG. 13. Photographs showing the projected states of the reticle for fixed target tracking and the reticle for the moving target tracking used on two adjacent sides of the cubic beam-splitter.

FIG. 14. Photographs depicting how an external object and virtual image of the reticle can be seen in a superimposed state anywhere on the observation window in the developed optical sighting system.

window of the optical sighting system is given, and how much the horizontal and vertical rotation angles of the FSM are required to have a specific leading angle, has not been the developed. But in this paper, we could solve these problems.

Also, by using a cubic beam-splitter, this optical sighting system can have a wider leading angle than conventional optical sighting systems.

With this program, we have confirmed that the achievable maximum leading angle is in a range of ±11.7° when the FSM is horizontally driven to ±18.5° and the maximum horizontal leading angle has a range of about ±8.2° with the maximum horizontal driving angle ($\beta = \pm 12.5°$) of the currently adopted FSM. Also, if diagonal leading angles are allowed, we confirmed that a β horizontal driving angle of ±12.5° and α vertical driving angle of ±7.1° can achieve a diagonal leading angle of ±10.0°.

In the future, we hope that the optical sighting system we developed, which is capable of producing a larger leading angle as described above, will be widely used as the optical sighting system of the Vulcan and others.

ACKNOWLEDGMENT

This work was supported by a 2017 Far East University Research Grant (FEU2017S09).

REFERENCES

1. J. A. Cameron and D. L. Fraley, "Apparatus for boresighting a firearm," U.S. Patent 5001836 (1991).
2. L. E. Moore and A. Moore, "Gun with mounted sighting device," U.S. Patent 0209381 A1 (2011).
3. S. H. Park, B. S. Jung, and D. H. Lee, "Development of prism dot-sight combined with thermal imaging camera," J. Korean Ophthalmic Opt. Soc. **19**, 479-485 (2014).
4. D. H. Lee, B. S. Jung, and S. H. Park, "Development of dot sight with prism beam splitter," J. Korean Ophthalmic Opt. Soc. **18**, 519-524 (2013).
5. D. H. Lee and S. H. Park, "Development of dot sight with 2X magnification," J. Korean Ophthalmic Opt. Soc. **17**, 435-440 (2012).
6. D. H. Lee, "Development of day and night scope with BS prism," J. Korean Ophthalmic Opt. Soc. **19**, 339-344 (2014).
7. L. R. Hedding and R. A. Lewis, "Fast steering mirror design and performance for stabilization and single axis scanning," Proc. SPIE **1304**, 14-24 (2005).
8. Q. Wang, K. Chen, and C. Y. Fu, "Method for controlling fast-steering mirror driven by voice coil motor based on the closed-loop performance," Opto-Electron. Eng. **32**, 9-11 (2005).
9. M. J. Xie, J. G. Ma, and C. Y. Fu, "Design and experiment of a LQ controller used in high-bandwidth fast-steering mirror system," Proc. SPIE **4025**, 250 (2000).
10. H. F. Mokbel, W. Yuan, L. Q. Ying, C. G. Hua, and A. A. Roshdy, "Research on the mechanical design of two-axis fast steering mirror for optical beam guidance," in *Proc. 2012 International Conference on Mechanical Engineering and Material Science* (China, Dec. 2012), pp. 205-209.
11. G. B. Arfken and H. J. Weber, *Mathematical Methods for Physicists 6th ed.* (Elsevier Academic Press, NY, USA, 2005), pp. 202-203.
12. G. G. Slabaugh, *Computing Euler angles from a rotation matrix*, http://citeseerx.ist.psu.edu/viewdoc/download?doi=10.1.1.371.6578&rep=rep1&type=pdf
13. K. Shoemake, "Animating rotation with quaternion curves," in *Proc. SIGGRAPH '85 Proceedings of the 12th Annual Conference on Computer Graphics and Interactive Techniques* (USA, Jul. 1985), pp. 245-254.
14. E. Kovács, "Rotation about an arbitrary axis and reflection through an arbitrary plane," Ann. Math. Inform. **40**, 175-186 (2012).
15. J. H. Burge, "Introductory Optomechanical Engineering, 6. Mirror matrices," *Optical Sciences 421/521, University of Arizona*, https://wp.optics.arizona.edu/optomech/wp-content/uploads/sites/53/2016/08/6-Mirror-matrices.pdf
16. R. E. Fischer and B. Tadis-Galeb, *Optical System Design 2nd Ed.* (McGraw-HILL, NY, USA, 2008), pp. 758-759.
17. P. M. Lund, "Optical element of a parallax free sight," U.S. Patent 5440387 (1995).